Next Generation NASA Hazard Detection System Development

Carolina I. Restrepo *
NASA Goddard Spaceflight Center, Greenbelt, MD, 20771

Po-Ting Chen †
Jet Propulsion Laboratory, California Institute of Technology, Pasadena, CA, 91109

Ronald R. Sostaric ‡, John M. Carson III §
NASA Johnson Space Center, Houston, TX

The SPLICE project is continuing NASA's efforts to develop precision landing GN&C technologies for future lander missions. One of those technologies is the next generation Hazard Detection (HD) System, which consists of a new HD Lidar and HD Algorithms. The HD System is a modular system that will be adapted to meet specific mission needs in the future. This paper presents the design approach, the nominal concept of operations for which the first prototype is being designed, and the expected performance of the system.

I. Introduction

Guidance, Navigation and Control (GN&C) technologies for precise and safe landing are essential for future robotic science and human exploration missions to various solar system destinations. These Entry, Descent and Landing (EDL) technologies are a part of NASA's Precision Landing and Hazard Avoidance (PL&HA) domain, and are considered high-priority capabilities for space technology development roadmaps [1] to promote and enable new mission concepts. The SPLICE project, or Safe & Precise Landing - Integrated Capabilities Evolution [2], is focusing on the continued development of sensors, algorithms, and avionics for infusion into future lunar landing missions. Specifically, SPLICE is maturing the Technology Readiness Level (TRL) of sensor hardware and software for both Terrain Relative Navigation (TRN) and Hazard Detection and Avoidance (HDA) during a lander's descent. All of the work on SPLICE is heavily based on previous NASA projects within the PL&HA domain such as ALHAT [3–6], COBALT [7–10], LVS [11], which include multi-year sensor development efforts [12–15], and various sub-orbital flight tests.

SPLICE is a suite of GN&C technologies for precision landing. The individual components, listed in Table 1, can be flown separately or as an integrated payload hosted by a lander. The Navigation Doppler Lidar (NDL) developed at the NASA Langley Research Center provides cm-level precision velocity and ranging. The Hazard Detection Lidar (HDL) developed at the NASA Goddard Space Flight Center generates a high-resolution digital elevation map (DEM) of the area surrounding the intended landing target. The TRN system includes a camera, onboard maps and TRN algorithms which are being developed and implemented by the Charles Stark Draper Laboratory, Inc. for the SPLICE project [16]. The hazard detection algorithms developed at the NASA Jet Propulsion Laboratory are based on the ALHAT algorithms outlined in Ref. [17] with some modifications to work with the new HD Lidar DEMs and to run on the new Descent and Landing Computer (DLC). The DLC developed at the Johnson Space Center is a new avionics design that is being developed to leverage the High Performance Spaceflight Computing (HPSC) processor [18, 19].

Alongside the continued maturation of GN&C hardware and software for TRN and HDA, the project is also developing high-fidelity simulation environments including a hardware-in-the-loop (HWIL) testbed with the DLC and a few sensor emulators in the loop. Additionally, SPLICE is conducting detailed modeling of EDL architectures for robotic and human missions [20, 21] to establish future requirements, to reveal existing technology gaps, and to drive sensor technology development to benefit upcoming missions such as NASA's Artemis and Commercial Lander Payload Services (CLPS) programs.

Figure 1 is a high-level schematic of the SPLICE payload onboard a host vehicle. The image processing for TRN and HDA is computationally intensive, so the DLC is being designed to offload the primary flight computer by handling the bulk of the vision navigation algorithms. The flight software running on the DLC leverages the NASA core Flight

*Aerospace Engineer, Navigation and Mission Design Branch, AIAA Senior Member
†Member of Technical Staff, Guidance and Control Section
‡SPLICE Project Manager, AIAA Senior Member
§SPLICE Principal Investigator, AIAA Associate Fellow

Table 1 SPLICE Technologies

Sensors	Navigation Doppler Lidar Hazard Detection Lidar
Algorithms	Terrain Relative Navigation Hazard Detection 6DOF Guidance
Avionics	Descent & Landing Computer
Simulation	ConOps Studies for various reference missions
Integration & Test Capabilities	Hardware-in-the-loop Testbed PL&HA Lab (under development) Flight tests

System (cFS) architecture [22]. The software includes applications for all of the PL&HA sensor input/output interfaces, navigation filter and guidance applications, and a host vehicle I/O applications which transfer timing, navigation, and guidance solutions between the DLC and the primary flight computer. The dotted lines indicate that the Primary Flight Computer onboard the lander has the ultimate authority on whether or not accept/utilize the SPLICE payload navigation and/or guidance solutions.

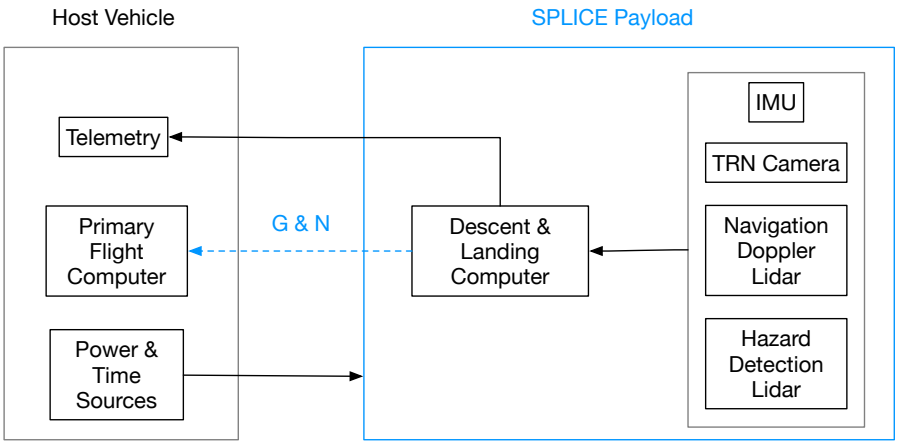

Fig. 1 SPLICE Technologies Onboard a Host Vehicle

SPLICE, just as previous PL&HA domain projects, has a few sub-orbital flight tests planned to increase the TRL level of its various components. While the project is focused on pushing TRL 3-6 technologies toward flight readiness, there is also a crucial need to continue the low-TRL (1-3) development of new research-level algorithms, which is being pursued through university partnerships. SPLICE is investing in advanced 6 Degree of Freedom (DOF) guidance algorithm development [23, 24], navigation filter design for EDL [25, 26], and the development of a lab at JSC that will allow testing of vision navigation algorithms indoors [27, 28] without the expense or risk of sub-orbital flight tests.

II. Notional Concept of Operations for Hazard Detection

The notional concept of operations for a lander with both TRN and HD systems onboard is shown in Fig. 2. The TRN system will likely start to operate from about 20 kilometers above the lunar surface. A optical camera on the lander takes 2-dimensional images of the surface, and the algorithms compare those images to rendered images of the area that the lander expects to see based on its navigation state. The image comparison allows the system to reduce its navigation errors by measuring the offsets between the actual and rendered imagery. These offset measurements (several per image frame) are sent to the navigation filter to update the navigation state. SPLICE and Draper developed and tested a version of this TRN system in 2019 [16].

The TRN system provides a lander with corrections to its global navigation state. However, the rendered surface maps for TRN are not of high enough resolution to help navigate the lander all the way to the surface nor to identify small cm-scale surface features that could damage the lander. A 3-dimensional DEM of the surface at much higher resolution is needed to accomplish hazard avoidance and hazard-relative navigation. The hazard detection system provides this map but it comes with an inherited global navigation state and associated errors from the TRN phase. The HD phase will likely start around 0.5 kilometers above the intended landing target. As shown in Fig. 2, the HD Lidar will generate a DEM of the surface relative to the sensor head but expressed in surface-fixed coordinates provided by the lander's navigation state. The HD algorithms will then characterize all the hazardous areas in the DEM and provide its host lander with options for safe landing sites. It is up to the lander's guidance system to chose one of the provided safe landing sites and to navigate towards it. The high-resolution DEMs will be suitable for performing hazard relative navigation in the future, which is a TRN-like function that utilizes the local maps to navigate. The SPLICE project currently does not have plans to develop or test hazard relative navigation, however this functionality was successfully tested during the ALHAT project with the Lidar DEMs.

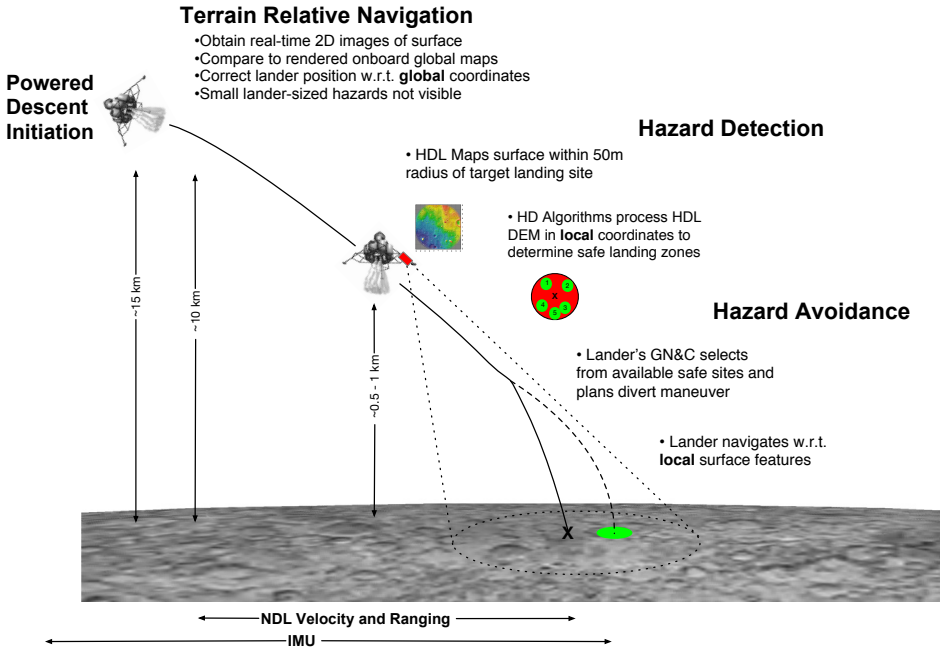

Fig. 2 Precision Landing & Hazard Avoidance ConOps

III. Hazard Detection System

The SPLICE HD System has two components: the HD Lidar and the HD algorithms for DEM analysis. As shown in Fig. 3, the inputs to the HD Lidar, which come from the host vehicle, are trajectory information (navigation state and state errors, propagated IMU states, and time) and commands to generate the DEM and transfer it to the DLC for map analysis and safe site selection. The instant the HD Lidar begins to scan the surface is defined as $t = 0$ and all subsequent range measurements are tied to the coordinate frame established at this time. In other words, the map that the HD Lidar generates is relative to its state at $t = 0$ and therefore, the DEM inherits the navigation errors from the state provided to the Lidar at that time. The HD Lidar is expected to generate the DEM in approximately 2 seconds, and its computer can transfer the DEM in Lidar-relative or surface-fixed coordinates to the DLC in approximately 1 additional second. The HD algorithms are expected to run on the DLC, and the safe site coordinates will be sent to the lander's primary flight computer for the main guidance system to consider.

The HD system design directly depends on the requirements placed on the quality of the DEM that must be generated in real-time and analyzed to detect safe landing locations. As shown in Fig. 4, the DEM quality drives the design of the sensor and the DEM generated drives the algorithm parameters along with constraints on the computing platform and the mission timeline.

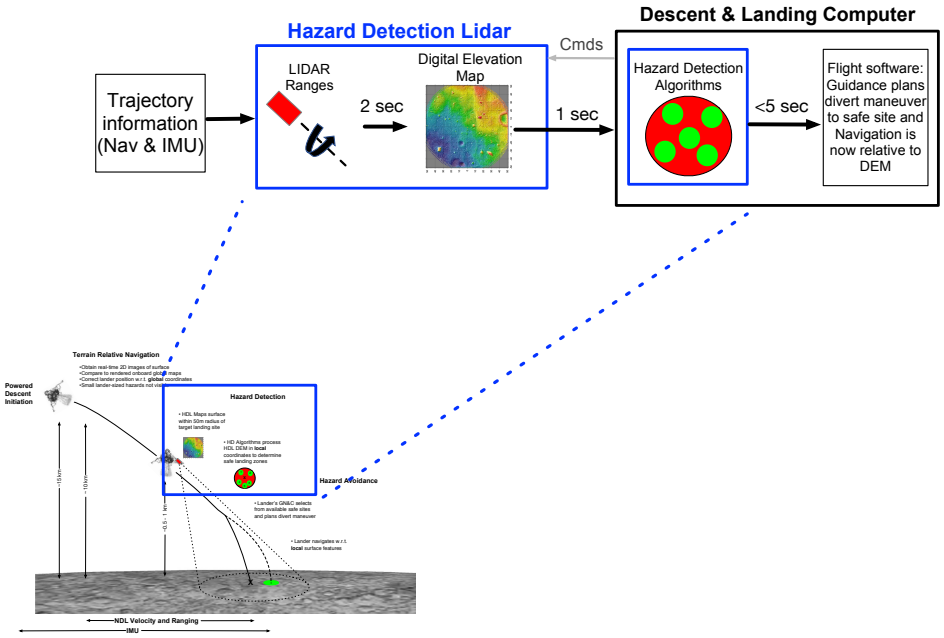

Fig. 3 SPLICE Hazard Detection System

Based on notional robotic lander concepts for NASA's CLPS missions and previous ALHAT project experience, the DEM quality must be such that 20 cm hazards and roughly 5° slopes can be identified. To properly map a 20 cm hazard, 2-3 pixels are necessary which implies that a resolution of approximately 5cm/pixel is needed. If a lander can tolerate larger hazards or steeper slopes, the DEM resolution requirements can be relaxed. For the first HD Lidar prototype, the SPLICE project has set specifications for the DEM quality as listed in Table 2.

Table 2 Specifications for DEM Quality

Map Size	100 $meter$ diameter circle centered at landing target
Ground Sample Distance	5 $cm/pixel$
DEM Elevation Errors	5 cm, $3-\sigma$
DEM Generation Time	2 seconds
DEM Transfer Time to DLC	1 second

Additionally, based on extensive simulation work to determine a realistic range of flight conditions in which the HD system might operate for various design reference missions, the first prototype of the SPLICE Lidar is being designed to operate within the flight conditions listed in Table 3, where slant range is defined as the shortest distance to the target and slant angle is defined as the angle between the slant range direction and the surface normal.

Table 3 Concept of Operations for HD

Slant range to landing target	400-600 m
Slant range angle	15° off nadir
Vertical velocity	10-40 m/s

To achieve coverage of the required surface area in 2 seconds, the current design consists of a hybrid imaging Lidar with an optical head and Risley prism scanning mechanism coupled to an electronics box that houses the laser and detectors. The design also includes an independent altimeter channel which is expected to provide altitude measurements well before the imaging Lidar starts to operate. The design includes various heritage parts from previous GSFC flight Lidars [2]. An engineering development unit (EDU) is being built and will be tested on an airborne platform in 2020.

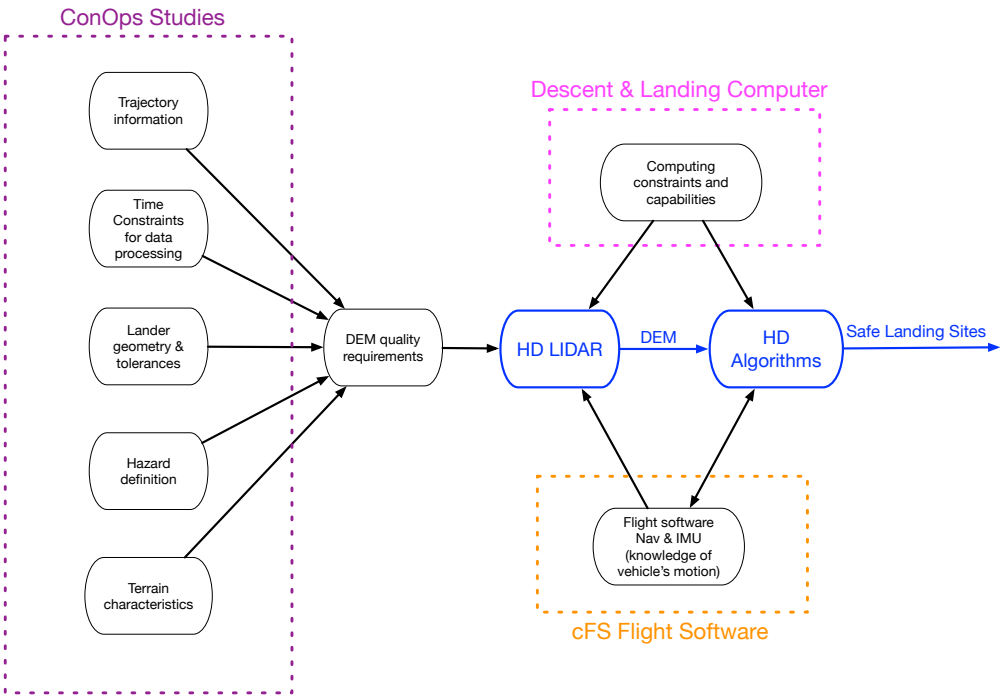

Fig. 4 HD System Drivers

IV. Hazard Detection Algorithms

The Hazard Detection algorithms being developed within SPLICE are directly leveraging the prior HD algorithms from the ALHAT project [17]. The HD algorithms take as inputs the lander geometry including the number and location of the leg pads. The code looks for hazards and slopes based on the interaction between the lander and the surface beneath. The hazard and slope information for each pixel underneath the lander is then combined with navigation uncertainties, as well as noise and errors from the DEM to ultimately provide the lander with a map of safe landing zones in a few seconds. The project plans to evaluate the HD algorithm performance both within the SPLICE HWIL simulation environment and with the data from the HD Lidar airborne test.

A low-fidelity HD System model has been developed at JPL and implemented in the POST2 Simulation [21] to understand the tight coupling between HD system design and mission concept of operations. An instantaneous Flash Lidar model (Fig. 5) performs ray-interception calculations to find the true ranges and it adds range noise and bias. The ranges are transformed into a point cloud in the local surface frame computed with lander state estimates. The point cloud is then binned into a grid to form the Lidar DEM. The DEM generation process is sensitive to the sensor Field of View (FOV), detector size, range noise and bias, grid dimensions, lander trajectory, scanning mechanism (pattern), and scanning duration.

The Lidar DEM is processed by the HD algorithms to produce a safety map. The HD algorithms process the DEM to assign a probability of a safe landing to each pixel on the map. The final safety map and safe site ranking that the algorithm produces is dependent on the lander vehicle size, lander footpad size, DEM elevation uncertainties, lander slope and roughness tolerances, touchdown dispersions, and the desired minimum safe site separation.

The number of holes in a DEM directly affects the areas of the map that can be considered safe since the algorithm's calculation of slope and roughness fails. The HD algorithm has the ability to "patch" single-pixel holes with information from the surrounding pixels, but if larger holes appear due to adjacent missing pixels, bad pixels or hazard shadows, the algorithm is conservative in nature and the safety map deteriorates quickly. If the Lidar DEM does not contain holes, the safety map remains relatively unchanged. To illustrate the ties between mission ConOps and the HD system, the following simple examples show the effects of two trajectory parameters: slant range and slant angle.

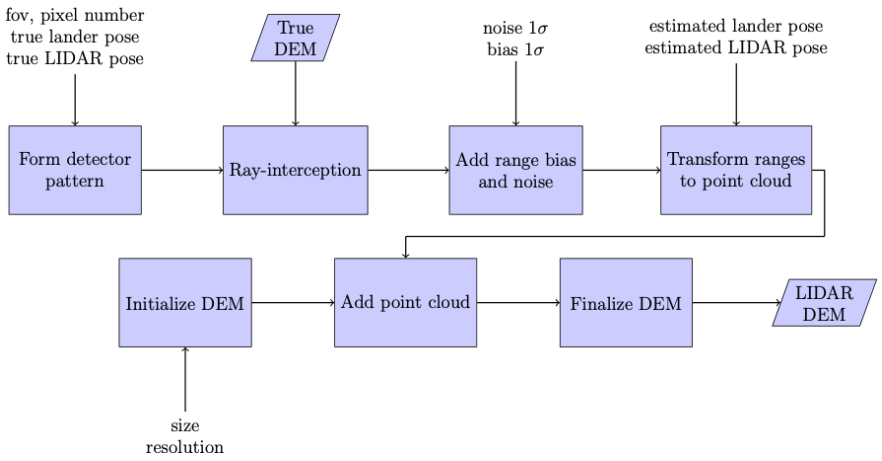

Fig. 5 Lidar-generated DEM Model

V. Examples

The examples use a synthetic DEM of the Apollo 12 landing site and Lidar DEMs generated with the process described in Fig. 5. A single-shot Lidar model is used in this analysis to take out the sensitivities induced by vehicle motion during HD Lidar scanning. The single-shot model is equivalent to a large pixel array Flash Lidar and not the ALHAT gimbaled Flash Lidar that generated a mosaic of range images. In this case, the number of pixels/detectors used is not representative of a particular Lidar hardware, but chosen to cover the 100 meter diameter map from an altitude of 500 meters.

Table 4 lists the simulation parameters and Fig. 6 shows the ground truth DEM and binary safety map. The binary safety map is the result of a pass/fail criteria for the lander's slope and roughness tolerances at each pixel. The binary safety map is combined with the lander's expected touchdown dispersions to calculate an overall probability of safe landing. This probability number is the value used to rank the safe sites before sending the top candidate sites to the host lander.

Table 4 Flash Lidar Model Parameters

Lidar DEM size: 100 x 100 m	Slant range: 500 - 1000 m	Lander leg pad radius: 20 cm
DEM Resolution: 0.05 cm	Slant angle: 65 - 90 deg	Lander vehicle radius: 3 m
Lidar Field of view: 11.4 deg	Minimum safe site separation: 10 m	Lander slope tolerance: 20 deg
Number of pixels: 1651 x 1651	Touchdown dispersion $1-\sigma$: 3 m	Lander roughness tolerance: 30 cm

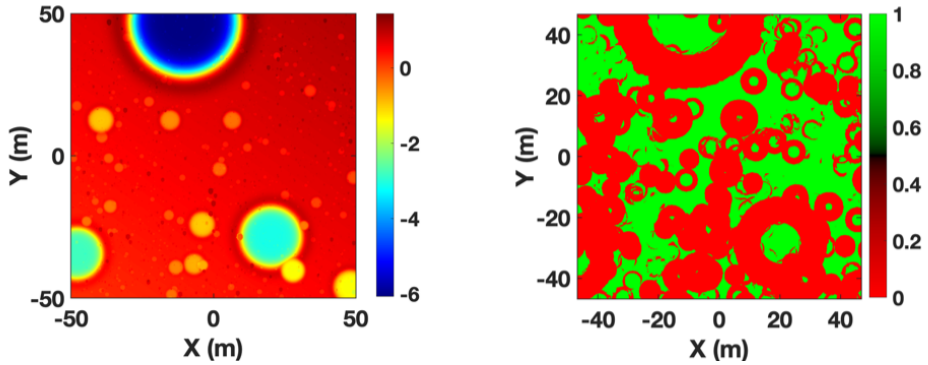

(a) Lidar DEM - no noise **(b) Binary Safety Map (Slope and Roughness)**

Fig. 6 Truth DEM and Binary Safety Map

A. Effects of Slant Angle

Figures 7-9 show a) Lidar DEM with noise, b) Slope map, c) Roughness map, and d) Combined slope, roughness, and touchdown dispersions into the overall safety probability map with the top safe sites. As the viewing angle of the surface deviates from nadir, holes in the map appear behind surface hazards. This sensitivity in slant angle would remain similar regardless of the Lidar hardware since DEM holes would still appear. The roughness calculation, which computed the height of the hazards that protrude above the plane formed by the lander's legs, cannot be completed with missing pixels. In this example, even though the safe sites chosen by the algorithm remain relatively unchanged, there are fewer safe areas in the map to choose from. Future studies will look at lower slant angles and results will help balance the constraints of having an HD system onboard with trajectory optimization constraints.

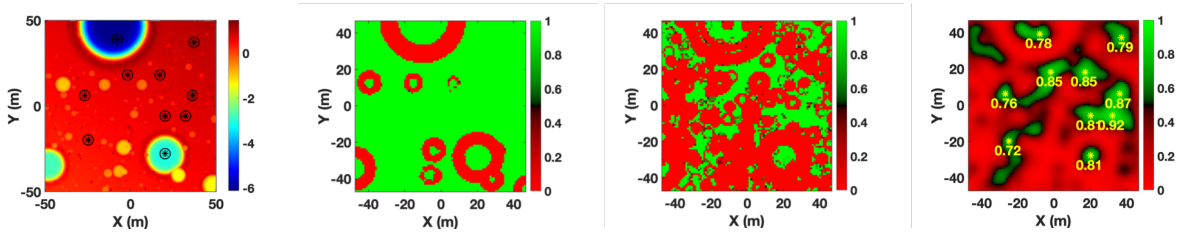

(a) Lidar DEM (b) Slope Map (c) Roughness Map (d) Safe Sites

Fig. 7 Slant Angle: 90deg, Slant Range: 500m

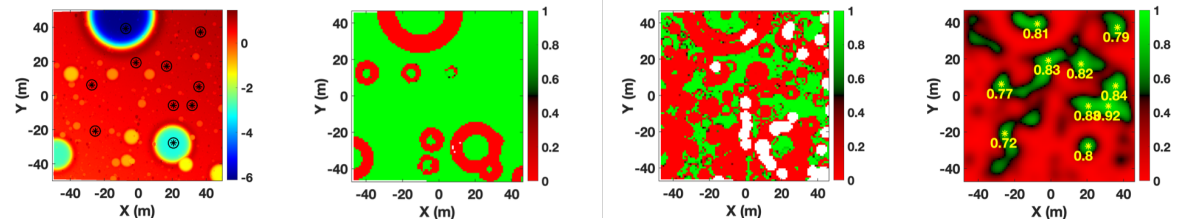

(a) Lidar DEM (b) Slope Map (c) Roughness Map (d) Safe Sites

Fig. 8 Slant Angle: 80deg, Slant Range: 500m

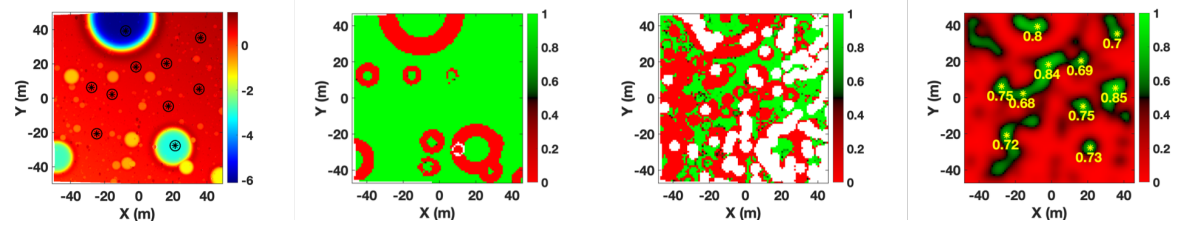

(a) Lidar DEM (b) Slope Map (c) Roughness Map (d) Safe Sites

Fig. 9 Slant Angle: 75deg, Slant Range: 500m

B. Effects of Slant Range

The sensitivity in slant range depends heavily on the number of detector pixels. The single-shot Flash Lidar model in this example has just enough pixels so that the 500 m vertical Lidar DEM does not have holes. The sensitivity would change depending on the Lidar hardware and DEM generation process. With increasing altitude, the number of detectors would also have to increase to preserve ground sample distance. Figures 10-12 show that the roughness calculation breaks down when the number of pixels is not enough to cover the surface since it can no longer identify the required minimum size hazards.

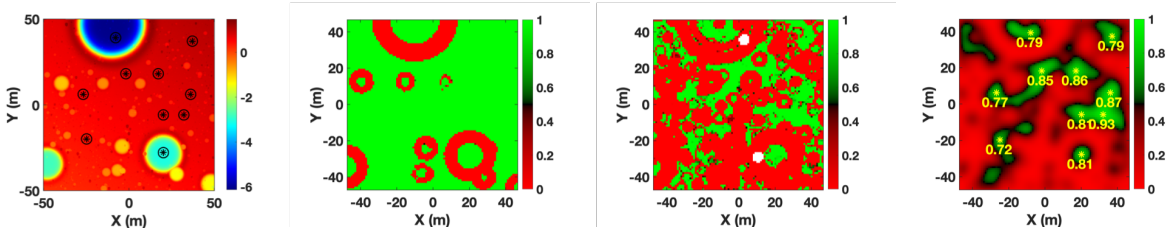

(a) Lidar DEM (b) Slope Map (c) Roughness Map (d) Safe Sites

Fig. 10 Slant Angle: 90deg, Slant Range: 600m

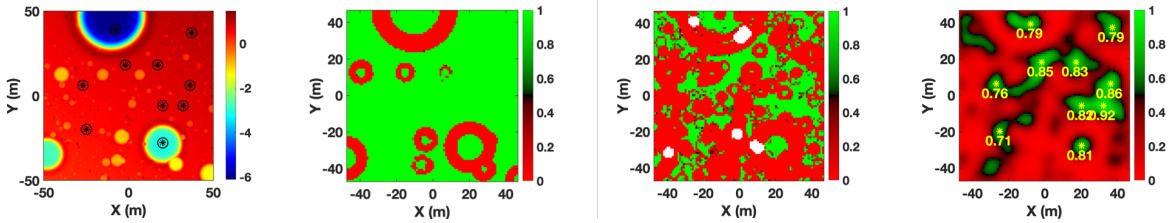

(a) Lidar DEM (b) Slope Map (c) Roughness Map (d) Safe Sites

Fig. 11 Slant Angle: 90deg, Slant Range: 700m

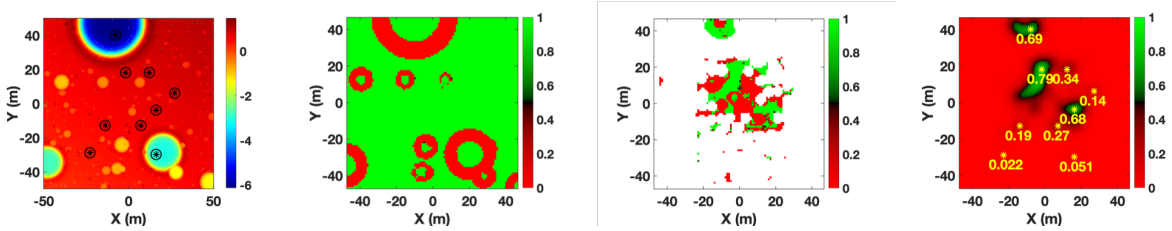

(a) Lidar DEM (b) Slope Map (c) Roughness Map (d) Safe Sites

Fig. 12 Slant Angle: 90deg, Slant Range: 800m

VI. Conclusion and Future Work

The HD System overall performance depends on various factors such as DEM generation process, lander geometry, trajectory and state knowledge errors, system timing, and the quality of all the sensors involved. Additionally, the HD System design is tightly coupled with mission ConOps. To ensure that the development of hazard detection and avoidance systems meets their future mission PL&HA needs, the project is currently engaged with the CLPS program, the Human Lander Systems program, as well as various commercial partners. Future work includes generation and analysis of high-fidelity and high-resolution terrains of various types to evaluate both the HD Lidar performance and HD algorithms, as well as porting the HD algorithm software into the DLC to evaluate it's real-time performance.

VII. Acknowledgements

The authors would like to thank the SPLICE team working on the integrated PL&HA system, the Entry Flight Mechanics team members at the NASA Langley Research Center for their help and insight into mission concept of operations for hazard detection, and the HD Lidar team at GSFC. The contributions to the HD algorithm work from the Jet Propulsion Laboratory, California Institute of Technology, were carried out under a contract with the National Aeronautics and Space Administration (80NM0018D0004).

References

[1] Office of the Chief Technologist, *2015 NASA Technology Roadmaps*, NASA, 2015. URL `http://www.nasa.gov/offices/oct/home/roadmaps/index.html`.

[2] Carson III, J. M., Munk, M. M., Sostaric, R. R., Estes, J. N., Amzajerdian, F., Blair, J. B., Rutishauser, D. K., Restrepo, C. I., Dwyer-Cianciolo, A., Chen, G. T., and Tse, T., "The SPLICE Project: Continuing NASA Development of GN&C Technologies for Safe and Precise Landing," *AIAA Scitech Forum*, San Diego, CA, 2019.

[3] Rutishauser, D. K., Epp, C. D., and Robertson, E. A., "Free-Flight Terrestrial Rocket Lander Demonstration for NASA's Autonomous Landing and Hazard Avoidance Technology (ALHAT) System," *Proc. AIAA SPACE 2012 Conference & Exposition*, 2012.

[4] Epp, C. D., Robertson, E. A., and Carson III, J. M., "Developing Autonomous Precision Landing and Hazard Avoidance Technology from Concept through Flight-Tested Prototypes," *Proc. AIAA GN&C Conference*, Kissimmee, FL, 2015.

[5] Carson III, J. M., Robertson, E. A., Pierrottet, D. F., Roback, V. E., Trawny, N., Devolites, J. L., Hart, J. J., Estes, J. N., and Gaddis, G. S., "Preparation and Integration of ALHAT Precision Landing Technology for Morpheus Flight Testing," *Proc. AIAA Space 2014 Conference & Exposition*, San Diego, CA, 2014. doi:doi:10.2514/6.2014-4313.

[6] Carson III, J. M., Hirsh, R. L., Roback, V. E., Villalpando, C. Y., Busa, J. L., Pierrottet, D. F., Trawny, N., Martin, K. E., and Hines, G. D., "Interfacing and Verifying ALHAT Safe Precision Landing Systems with the Morpheus Vehicle," *Proc. AIAA GN&C Conference*, Kissimmee, FL, 2015.

[7] Carson III, J. M., Seubert, C. R., Amzajerdian, F., Villalpando, C. Y., Bergh, C., O'Neal, T., Robertson, E. A., Hines, G. D., and Pierrottet, D. F., "COBALT: a Payload for Closed-Loop Flight Testing of ALHAT GN&C Technologies on Terrestrial Rockets," *Proc. AIAA Space 2016 Conference & Exposition*, Long Beach, CA, 2016.

[8] Carson III, J. M., Seubert, C. R., Amzajerdian, F., Bergh, C., Kourchians, A., Restrepo, C. I., Villalpando, C. Y., O'Neal, T., Robertson, E. A., Pierrottet, D. F., Hines, G. D., and Garcia, R., "COBALT: Development of a Platform to Flight Test Lander GN&C Technologies on Suborbital Rockets," *Proc. AIAA 2017 SciTech/GN&C Conference*, Grapevine, TX, 2017.

[9] Carson III, J. M., Restrepo, C. I., Seubert, C. R., Amzajerdian, F., Pierrottet, D. F., Collins, S. M., O'Neal, T., and Stelling, R., "Open-Loop Flight Testing of COBALT Navigation and Sensor Technologies for Precise Soft Landing," *Proc. AIAA SPACE 2017 Conference & Exposition*, Orlando, FL, 2017.

[10] Restrepo, C. I., Carson III, J. M., Amzajerdian, F., Seubert, C. R., Lovelace, R., McCarthy, M. M., Tse, T., Stelling, R., and Collins, S. M., "Open-Loop Performance of COBALT Precision Landing Payload on a Commercial Sub-Orbital Rocket," *AIAA Scitech Forum*, Kissimmee, FL, 2018.

[11] Johnson, A., Bergh, C., Cheng, Y., et al., "Design and Ground Test Results for the Lander Vision System," *36^{th} Annual AAS Guidance and Control Conference*, Breckenridge, CO, 2013.

[12] Pierrottet, D. F., Hines, G. D., Barnes, B. W., Amzajerdian, F., Petway, L. B., and Carson III, J. M., "Navigation Doppler Lidar Integrated Testing Aboard Autonomous Rocket Powered Vehicles," *Proc. AIAA 2018 SciTech/GN&C Conference*, 2018.

[13] Amzajerdian, F., Pierrottet, D. F., Petway, L. B., Hines, G. D., Roback, V. E., and Reisse, R. A., "Lidar Sensors for Autonomous Landing and Hazard Avoidance," *Proc. AIAA SPACE 2013 Conference & Exposition*, San Diego, CA, 2013.

[14] Amzajerdian, F., Hines, G. D., Petway, L. B., Barnes, B. W., and Pierrottet, D. F., "Development and Demonstration of Navigation Doppler Lidar for Future Landing Mission," *Proc. AIAA Space 2016 Conference & Exposition*, Long Beach, CA, 2016.

[15] Johnson, A., Keim, J., and Ivanov, T., "Analysis of Flash Lidar Data Field Test Data for Safe Lunar Landing," *Proc. IEEE Aerospace Conference (AEROCONF 2010)*, 2010.

[16] Fritz, M. P., Olguin, A. S., Smith, K. W., Lovelace, R., Sostaric, R., Pedrotty, S., Estes, J. N., Tse, T., and Garcia, R., "Operational Constraint Analysis of Terrain Relative Navigation for Landing Applications," *AIAA Scitech Forum*, Orlando, FL, 2020.

[17] Ivanov, T., Huertas, A., and Carson, J., "Probabilistic Hazard Detection for Autonomous Safe Landing," *Proc. AIAA Guidance, Navigation, and Control Conference*, 2013.

[18] Rutishauser, D. K., Moore, R., Prothro, J., and Yim, H., "High-Performance Computing for Precision Landing and Hazard Avoidance and Co-design Approach," *IEEE Aerospace Conference*, Big Sky, MT, 2019.

[19] Rutishauser, D. K., and Tse, T., "Hardware-in-the-Loop Testing for Suborbital FLights of the Safe and Precise Landing Integrated Capabilities Evolution (SPLICE) Project," *AIAA Scitech Forum*, Orlando, FL, 2020.

[20] Dwyer-Cianciolo, A., Striepe, S., Carson III, J. M., Sostaric, R. R., Woffinden, D., Karlgaard, C., Lugo, R., Powell, R., and Tynis, J., "Defining Navigation Requirements for Future Precision Lander Missions," *AIAA Scitech Forum*, San Diego, CA, 2019.

[21] Dwyer-Cianciolo, A., Dutta, S., Lugo, R., Williams, A., and Chen, P.-T., "A Simulation Framework for Precision Landing and Hazard Avoidance Technology Assessments," *AIAA Scitech Forum*, Orlando, FL, 2020.

[22] NASA, *Core Flight Software*, Goddard Spaceflight Center, 2019. URL `https://cfs.gsfc.nasa.gov/`.

[23] Reynolds, T. P., Szmuk, M., Malyuta, D., Mesbahi, M., Açikmeşe, B., and Carson III, J. M., "A State-Triggered Line of Sight Constraint for 6-DoF Powered Descent Guidance Problems," *AIAA Scitech Forum*, San Diego, CA, 2019.

[24] Reynolds, T. P., Malyuta, D., Szmuk, M., Mesbahi, M., Açikmeşe, B., and Carson III, J. M., "Numerical Verification of Optimal 6-DoF Powered Descent Guidance," *AIAA Scitech Forum*, Orlando, FL, 2020.

[25] Burke, J. D., and DeMars, K. J., "Uncertainty Propagation for Coning, Sculling, and Scrolling Algorithms for Descent-to-Landing Navigation," *AIAA Scitech Forum*, Orlando, FL, 2020.

[26] Ward, K. C., and DeMars, K. J., "Impact of Considering and Neglecting States on Descent-to-Landing Navigation," *AIAA Scitech Forum*, Orlando, FL, 2020.

[27] Majji, M., Simon, A. B., Restrepo, C. I., and Lovelace, R., "A Comparison of Feature Extraction Methods for Terrain Relative Navigation," *AIAA Scitech Forum*, Orlando, FL, 2020.

[28] Simon, A. B., Majji, M., Restrepo, C. I., and Lovelace, R., "Navigation, Estimation, and Sensing Testbed (NEST) for Laboratory Validation of Algorithms," *AIAA Scitech Forum*, Orlando, FL, 2020.